Experimental characterization of combustion instabilities in high-mass-flux hybrid rocket engines

Fraters, A; Cervone, A

DOI
10.2514/1.B35485

Publication date
2016

Document Version
Accepted author manuscript

Published in
Journal of Propulsion and Power: devoted to aerospace propulsion and power

Experimental Characterization of Combustion Instabilities in High Mass Flux Hybrid Rocket Engines

Arjan Fraters[1] and Angelo Cervone[2]
Delft University of Technology, Delft, The Netherlands

A test campaign to characterize the performance, combustion behavior and blow-off limit at high mass flux levels of a particular hybrid rocket engine is presented and discussed. The test engine has a nominal thrust level of 300 N, with nitrous oxide (N_2O) as oxidizer and polymethyl methacrylate (PMMA) as solid fuel. A total of fifteen burns have been performed, at three different initial oxidizer mass flux levels: below, around and above the 500-700 kg/s·m^2 range with a maximum tested mass flux higher than 1300 kg/s·m^2. No complete blow-off has been observed in the high mass flux regime; however, combustion instabilities and spontaneous engine operation shifting, leading to lower combustion efficiency, have been noticed. These phenomena have been analyzed and compared to the theoretical models available in open literature. With the knowledge obtained from the test campaign, the observed low efficiency unstable behavior can effectively be prevented in future engines operating at high mass flux.

Nomenclature

CR	=	average combustion roughness [%]
$D_{p,i}$	=	initial port diameter [mm]
D_t	=	nozzle throat diameter [mm]
$G_{ox,i}$	=	initial oxidizer mass flux [kg/s·m^2]
L_p	=	port length [mm]
m_{ox}	=	oxidizer mass flow [g/s]
m_{fu}	=	fuel mass flow [g/s]
O/F	=	oxidizer-to-fuel mass ratio [-]

[1] M.Sc. student, Space Systems Engineering, Aerospace Engineering Faculty, Kluyverweg 1, 2629 HS Delft.
[2] Senior Lecturer, Space Systems Engineering, Aerospace Engineering Faculty, Kluyverweg 1, 2629 HS Delft.

p_c = combustion pressure [bar]

η_{c^*} = c* efficiency [-]

I. Introduction

HYBRID rocket engines, especially smaller ones such as those used in amateur rocketry, are generally operated at mass flux levels lower than 500 kg/s·m^2 [1]. As a general "rule of thumb" for their design, literature references typically mention values in the range of 500 to 700 kg/s·m^2 as the maximum attainable design mass flux level [2–6]. Although these mass flux levels are usually acceptable for small engines, in larger ones such as the 11 MN rocket of the Hybrid Propulsion Technology program [7] and the Stanford 66.7 kN Peregrine engine [6] it is very attractive (and sometimes even necessary) to operate at a higher initial mass flux, possibly in a range of 1100 to 1300 kg/s·m^2, in order to achieve a sufficiently high volumetric efficiency. In most of the publications mentioning a maximum design mass flux value, no convincing explanation is given on the way this value has been derived and under which assumptions. However, a recent publication on the development of the Peregrine engine [6] provides actual test data showing that no stable combustion could be obtained above a mass flux level of 650 kg/s·m^2. The authors claim that by implementing an improved injector design, stable combustion would also be obtained with higher mass flux levels.

A 10 kN hybrid rocket engine is currently being developed by students of the Delft University of Technology [8]. The project aims to deliver a 15 kg scientific payload to an altitude of 50 km. During the design phase of the engine, it was necessary to reduce the initial oxidizer mass flux from 1100 to 600 kg/s·m^2 in order to avoid combustion instabilities. These design changes were indeed successful, since in the first test campaign the engine operated stably. However, to understand if and how it would be possible for future projects to achieve stable operation at higher initial mass flux levels, a test campaign has been conducted to study the performance and combustion behavior of hybrid engines as functions of the oxidizer mass flux. This paper provides an overview of the methodology and experimental setup used during the test campaign, as well as the main results obtained from it.

II. Theoretical Background

The main effect of increasing the oxidizer mass flux in a hybrid rocket is the occurrence of problems such as flame holding and combustion instabilities (usually in combination with lower combustion efficiency), eventually followed by complete blow-off of the flame.

Combustion instability and low combustion efficiency have been observed at mass flux levels above 650 kg/s·m^2 in N_2O-paraffin hybrid rockets at both laboratory scale and full-scale items such as the Peregrine engine [6]. Blow-off is expected above a certain upper mass flux level which is inferred by the analysis conducted in several literature references on the flooding limit of hybrid rocket engines [7, 9–15]. However, it is still unclear how to quantify this upper mass flux level and what are the critical design factors influencing it, with different references even providing contradictory information in this respect. Furthermore, this upper mass flux limit is usually studied by means of analytical or semi-empirical models and little experimental data are available.

However, more literature can be found on a similar type of device, the solid fuel ramjet, in particular in studies dedicated to its upper flammability limit [16–19]. These papers provide experimentally determined upper mass flux limits as functions of several design parameters. It is clearly shown that the presence of a recirculating flow at the front of the fuel grain is critical for achieving a high upper flammability limit. This flow exchanges heat with the incoming oxidizer and transports fuel to the leading edge of the flame sheet, helping the flame to be stably attached to that point of the grain. At the upper flammability limit, the time for the reactants to mix and react inside the recirculating flow becomes too short to stabilize the flame. This limit is often provided in terms of a critical value of the Damköhler number, defined as the ratio of residence time (inside the recirculating flow in this case) to the time it takes for the reactants to mix and react.

The importance of achieving better flame stability in front of the fuel grain in hybrid rocket engines (recirculating flow) has been recognized in a study by Boardman et al. on combustion instabilities in an 11-inch diameter rocket engine [20, 21]. Their study confirms what is stated in the publication on the Peregrine rocket ground test results [6]: stable combustion at high mass flux levels should be possible by improving the injector design. However, what the “optimum” injector design is as a function of the other design parameters is currently unknown.

III. Methodology

From the literature overview presented, very few experimental data are available on the behavior of a hybrid rocket engine operating at increasing mass flux levels. For this reason, an experimental approach has been chosen for the present study.

The main goals of the experimental campaign were to find the blow-off limit for a given hybrid rocket engine configuration and to determine how its performance and combustion behavior (including the presence of possible instabilities) change when the initial oxidizer mass flux increases. The tests were performed at three different initial mass flux levels: below, around and above the 500-700 kg/s·m^2 range, up to more than 1300 kg/s·m^2.

In this study, the required variation of initial oxidizer mass flux has been achieved by varying the initial port diameter of the solid fuel grain of hollow cylindrical shape, while keeping the injector design and the oxidizer mass flow constant. This method also ensures that the observed difference in performance and combustion behavior are not due to changes in the injector pressure and in the way the oxidizer is injected into the chamber. A drawback, however, is that the initial volume available for the recirculating flow in the pre-combustion chamber differs as a consequence of the different initial port diameter: this effect will be taken into account when interpreting the results.

Liquid nitrous oxide has been used as oxidizer for safety reasons but also to gain greater insight into the propulsive performance of this type of propellant. PMMA (polymethyl methacrylate) has been selected as fuel, due mainly to its transparency, which makes visual observation of the ignition process possible.

IV. Test Setup and Procedures

A laboratory-scale hybrid engine test setup (Fig. 1) was used for the experimental campaign. The left stand visible in Fig. 1 holds the oxidizer tank and part of the feed system, while the right stand holds the combustion chamber with the other parts of the feed system on top of it, as well as the control electronics.

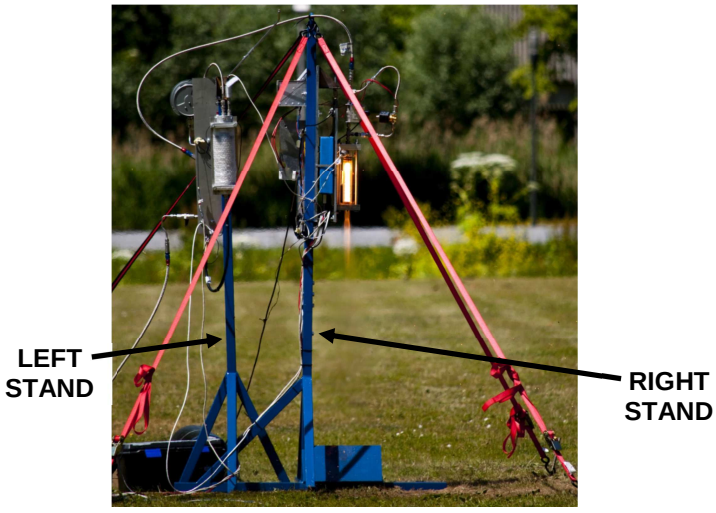

Fig. 1 Photo of the test setup during engine firing

A. Combustion Chamber

The layout of the combustion chamber is shown in Fig. 2 and in the section view to the right, where the main components are denoted by numbers. Component (1) is an aluminum injector body with a pressure tap to the injector manifold in its left side, and a pressure tap to the pre-combustion chamber in its right side. The aluminum injector plate (2) is attached to the component (1) by means of screws and sealed by a Teflon ring. Component (3) is the actual PMMA combustion chamber, which also acts as fuel. It includes a pre-combustion chamber just downstream the injector, into which the igniter (a squib made of black powder and steel wool) is placed. Component (4) is a Isographite M 40 nozzle, held in place by a steel nozzle sleeve (5). Sealing of the injector and the nozzle is done by means of O-rings protected by bearing grease.

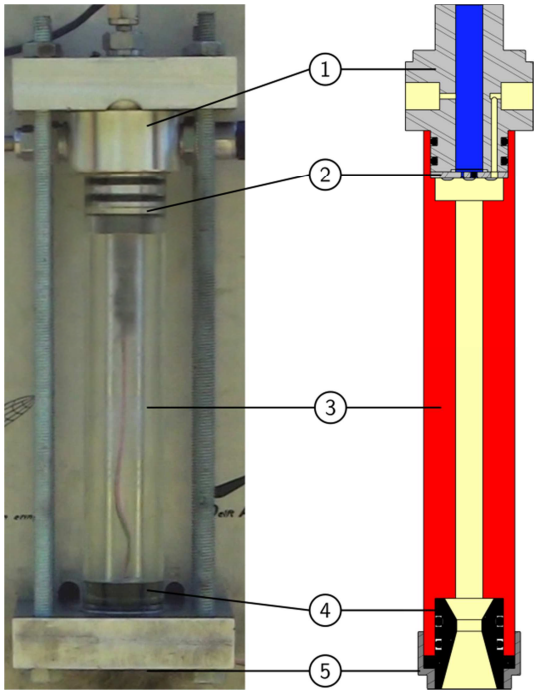

Fig. 2 Combustion chamber layout: photo of the assembled hardware before one of the tests (left) and section view of the chamber (right)

B. Feeding System

The feeding system layout is schematically shown in Fig. 3. A nitrogen cylinder can be connected to the test rig before or after the experiments, for operations such as pressure/leak-testing or system purging with gas at 60 bar. During the actual experiments, however, a N_2O cylinder is connected to the test rig. Before each test, the run tank is filled with liquid N_2O up to 80% of its capacity. This is done by first opening the fill valve (FV) with all other

valves closed and then opening the bleed valve (BV) exiting to the atmosphere through a long pipe. The bleed valve and fill valve are closed again when the liquid in the run tank has reached the required level. Then the run tank is heated by a heating wire wrapped around it, until the nitrous oxide reaches the test pressure of 60 bar. To start a test, first the safety valve (SV) is opened; then the igniter valve (IV) is opened for about 3 seconds in order to deliver a small amount of propellant to the chamber by means of a flow regulator (FR), which then reacts with the activated igniter and heats up the chamber. Finally, the main valve (MV) is opened to start the main oxidizer flow and fire the engine at its full thrust level. After 2.5 seconds the main valve and the ignition valve are closed, and the remaining oxidizer in the tank and feeding system is purged by opening the bleed valve. An analog pressure gauge (APS) and a pressure relief valve (PRV) are connected to the top bulkhead of the run tank as additional safety devices.

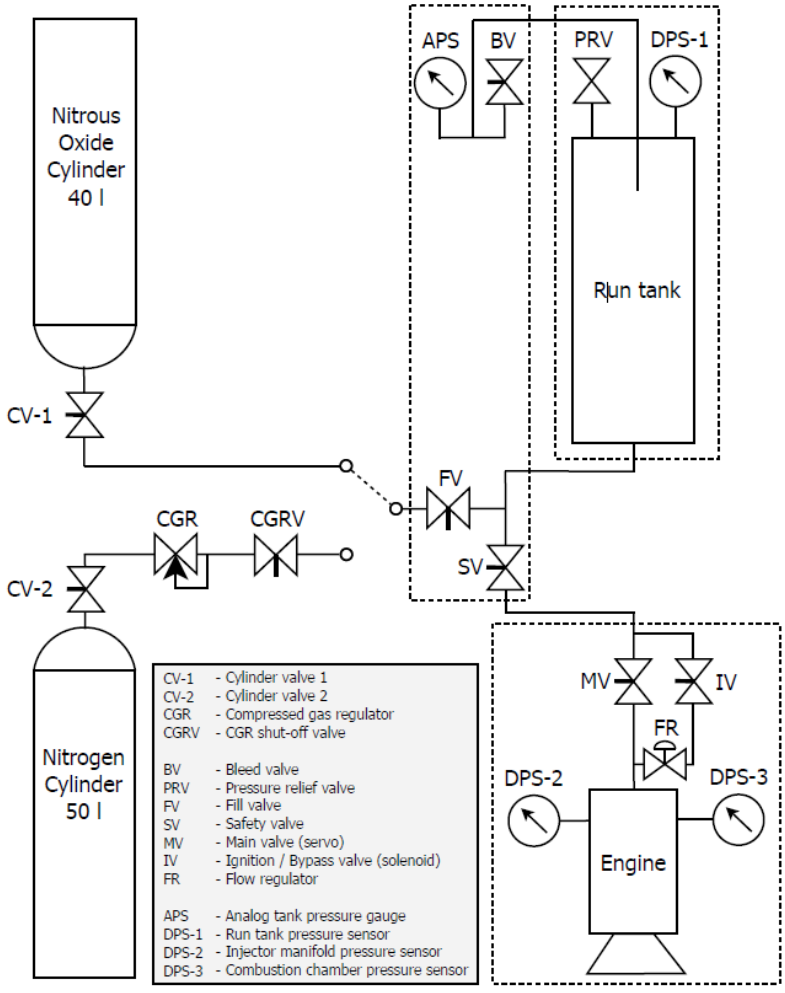

Fig. 3 Piping and instrumentation diagram of the feeding system

C. Sensors, Data Acquisition and Control System

To characterize the performance and combustion behavior of the engine, two load cells (not shown in Fig. 3) and three digital pressure sensors (denoted by DPS in Fig. 3) are incorporated into the test setup. The first load cell, a 111 N (25 lbf) Feteris FLLSB200 S-beam junior load cell with an accuracy of 0.1% of the rated output, is used to measure the tank weight. The second, a 100 kgf Scaime ZFA S-beam load cell with an accuracy of 0.05% of the rated output, measures the thrust. Two of the pressure sensors, model Honeywell 13C1000PA4K (1000 psi full scale, accuracy 0.1% of the rated output) are used to measure the run tank pressure (DPS-1) and the injector upstream pressure (DPS-2). The third pressure sensor, model Parker ASIC (100 bar full scale, accuracy 0.05% of full-scale output), measures the combustion pressure (DPS-3).

Two different devices are used for data acquisition. The load cells signals, as well as those from the pressure sensors DPS-1 and DPS-2, are recorded by a DATAQ DI-710-ULS 14-bit data logger, each with a relatively slow sample rate of 225 Hz. The combustion pressure from sensor DPS-3 is recorded by a NI USB-6211 16-bit system, at a sampling rate of 2200 Hz. The combustion chamber is filmed by two high-definition cameras and one for close-up videos of the combustion chamber at 240 fps.

The control system is located in the electronics box on the engine stand. It is used to switch the run tank heating system on and off, open and close the servo actuated valve MV and the igniter valve IV, and activate the igniter. The control system can be accessed and programmed from a distance of 50 m, with a laptop and a custom-developed Java program. The firing sequence is run autonomously by the control electronics.

Table 1 shows, for the most important output quantities of the present study, the maximum estimated measurement uncertainty over all the tests presented in this paper. The data presented in the table have been obtained by means of the sensor accuracy, for quantities directly measured by sensors, or by combining the accuracies of different sensors and/or post-processing techniques, for quantities that are derived by measurements of multiple sensors or obtained as combinations of measurements with analytical/numerical derivations. Note, in particular, the relatively high uncertainty in the fuel mass flow rate and, consequently, in the mixture ratio. This is mainly caused by the large uncertainty of the method used for determining the fuel mass flow averaging time (see following section VI.A for more details).

Table 1 Estimated measurement uncertainty for some important output quantities (maximum values over all the tests)

Parameter	Maximum uncertainty
$D_{p,i}$	1.3%
D_t	1.5%
L_p	0.1%
p_c	0.1%
m_{ox}	4.6%
$G_{ox,i}$	4.8%
m_{fu}	29%
O/F	29.4%
η_{c^*}	7.2%

V. Test Matrix

Table 2 shows a total of 15 tests performed at initial mass flux levels between 330 and 1370 kg/s·m^2, with only a few providing useful data for successive analysis. In these tests, no complete flame blow-off occurred but, as it will be described in the next sections, several instabilities have been observed.

Three different injector configurations have been used to achieve the highest possible oxidizer mass flow (and hence mass flux) with the available test setup, as shown in Table 3 and Fig. 4. In particular, the three injectors shown in Fig. 4 are axial showerhead plates with 1 mm diameter holes and conical exit. The injector hole patterns of the first two plates have an outer diameter of 6 mm, while in the third one the outer diameter is 6.5 mm. The larger circles around the injector holes are the projections of the nozzle throat (dashed line), fuel ports (dotted lines), and pre-combustion chamber (dash-dot line). The pre-combustion chamber has a diameter of 30 mm and a length of 10 mm.

Table 2 Test matrix, including a summary of the most important test results

Test ID	Initial Port Diameter	Oxidizer Mass Flow	Initial Oxidizer Mass Flux	Fuel Mass Flow	Mixture Ratio	Chamber Pressure	Average Combustion Roughness	Combustion Efficiency	Comments
	$D_{p,i}$ [mm]	m_{ox} [g/s]	$G_{ox,i}$ [kg/s·m^2]	m_{fu} [g/s]	O/F [-]	p_c [bar]	CR [%]	η_{c^*} [-]	
1	21	114	330	14	7.9	23.4	1.4	0.99	
2	15	118	670	-	-	-	-	-	Combustion chamber failure
3	12	118	1040	15	8.0	21.3	2.2	0.88	
4	18	142	560	13	10.7	20.3	4.0	0.90	
5	12	146	1290	12	12.1	18.8	4.3	0.84	
6	12	-	-	-	-	-	-	-	Ignition system test
7	12	-	-	-	-	-	-	-	DAQ & ign. system failure
8	18	145	570	-	-	-	-	-	Ign. system failure
9	18	142	560	14	10.4	21.4	4.5	0.94	
10	12	142	1260	13	10.7	17.9	2.6	0.80	
11	20	142	450	-	-	-	-	-	Failed to ignite
12	13.5	140	980	15	9.6	20.3	3.5	0.89	
13	20	142	450	-	-	-	-	-	Failed to ignite
14	13.5	154	1080	13	11.4	21.7	8.4	0.91	
15	12	155	1370	16	9.9	21.7	8.6	0.87	

Table 3 Main engine geometry characteristics in the tests with the three injector configurations

Injector Type	Test ID	Initial Port Diameter	Nozzle Throat Diameter	Port Length
		$D_{p,i}$ [mm]	D_t [mm]	L_p [mm]
1	1, 2, 3	15 – 18 - 21	10	165
2	4, 5, 6, 7, 8, 9, 10, 11, 12, 13	12 – 13.5 – 18 - 20	11	175
3	14, 15	12 – 13.5	11	175

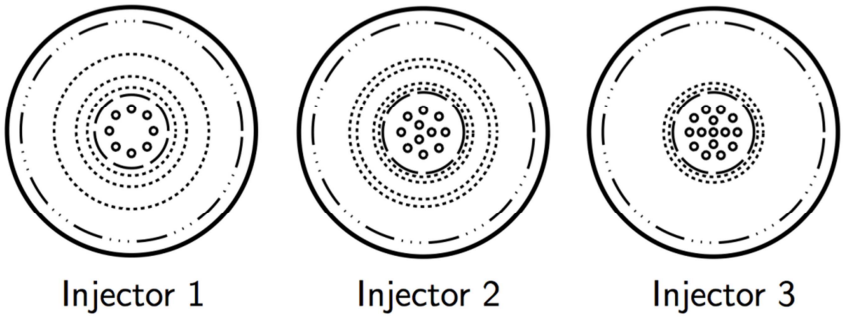

Fig. 4 Simplified front-view drawings of the three injector plates used during the test campaign, showing the different patterns of the 1 mm diameter holes in the center of each injector

VI. Results

Typical plots of the measured thrust, pressures and tank mass during a test are shown in Figs. 5 and 6 both from Test 12. Combustion pressure and thrust show a clear sudden shift in the downward (0.4 s after ignition) and upward direction (1.3 s after ignition) during the engine steady state operations. Similar shifting events have been observed in most of the other tests. Furthermore, none of these shifts show that the measured injector upstream pressure changes with such a magnitude to explain the large observed changes in combustion pressure (up to 6 bar in Test 12, as shown by Fig. 5). Any possible shift in the oxidizer mass flow is unfortunately difficult to detect because of the relative large noise in the tank mass. No significant difference in the average oxidizer mass flow has been found between tests with the same injector, but significantly different combustion pressure shifting behavior has been observed.

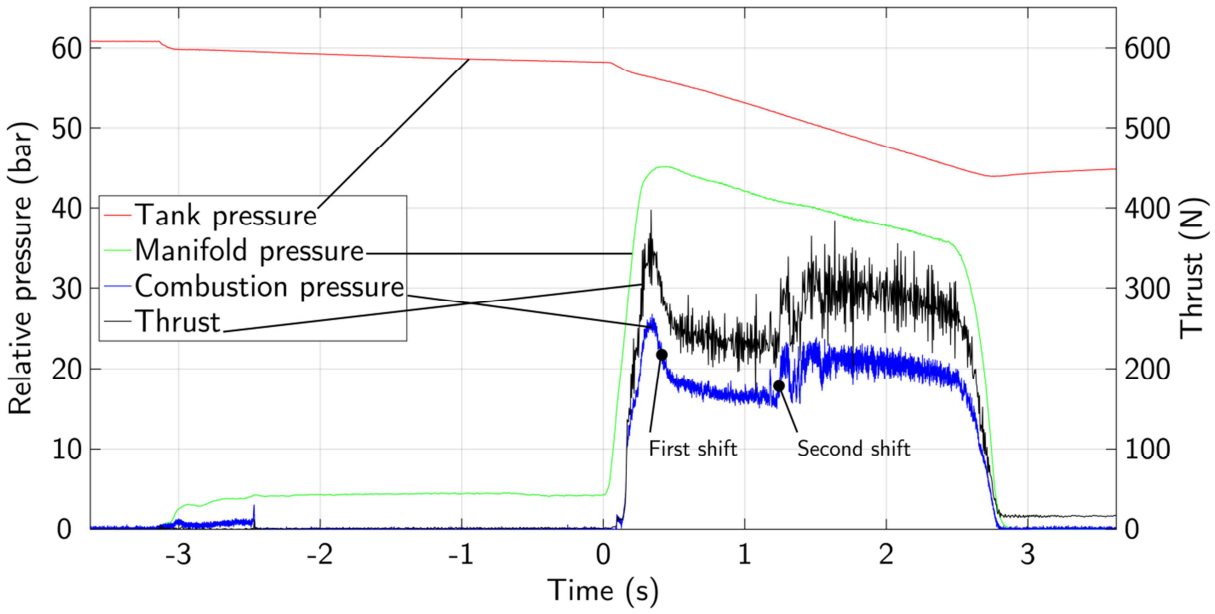

Fig. 5 Measured thrust and pressures in the tank, injector and chamber during Test 12, as functions of time

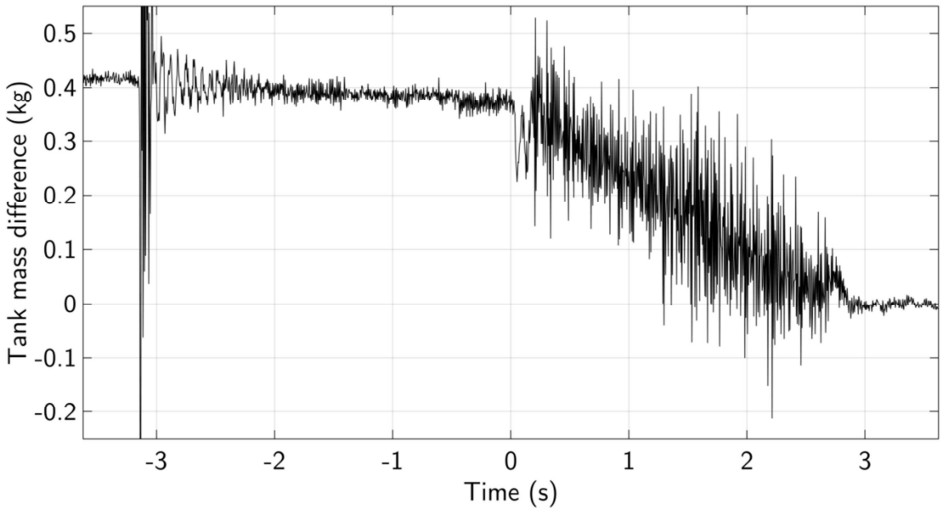

Fig. 6 Measured tank mass during Test 12, as a function of time

A. Engine Performance

For easier comparison of different tests, all measurements related to the engine performance have been averaged over the "steady state" operational time, defined as the time during which the feeding system pressure drop gradient is smaller than 10% of the maximum value (as shown in Fig. 7). The average oxidizer mass flow has been calculated by dividing the tank mass difference over a given burn by 2.67 s. This is the typical burn time during the

experimental campaign, as determined by analyzing the tank mass during all tests, in particular those in which the ignition failed and, hence, the tank mass data are much less noisy. The average fuel mass flow has been calculated by dividing the fuel grain mass change from before to after the test by an averaging time, defined as the time during which the combustion pressure is larger than 10% of its maximum value.

The initial oxidizer mass flux has been calculated dividing the average oxidizer mass flow by the initial fuel grain port diameter. It was unfortunately not possible to use direct measurements of the initial oxidizer mass flow rate, due to the poor quality of the instantaneous tank mass measurement data. However, at least some of the tests performed confirmed that this is an acceptable assumption, and no significant bias in the test results should be expected.

Lastly, the average experimental engine performance has finally been compared to the theoretically one. An overview of the most important results is given in Table 2.

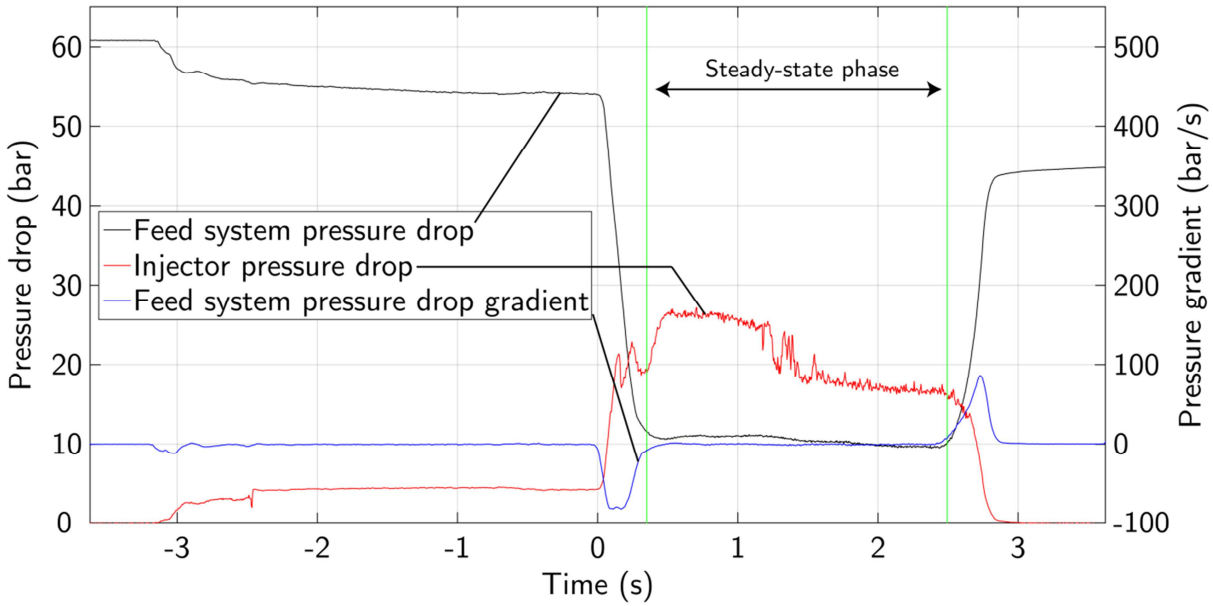

Fig. 7 Pressure drops over the feeding system and the injector for Test 12, as functions of time

B. Combustion Behavior and Instabilities

The main parameters used for analyzing the combustion behavior and the possible presence of instabilities are the combustion roughness and the combustion pressure frequency spectrum. The combustion roughness is defined as the absolute mean-to-peak combustion pressure difference as percentage of the local mean combustion pressure. A

typical combustion roughness graph is shown in Fig. 8 from Test 12. The average combustion roughness determined for each test is shown in Table 2, and seems to be unrelated to the initial mass flux. Typical Fast Fourier Transform plots of the combustion chamber pressure are shown in Fig. 9 and Fig. 10. Combustion instabilities in the range 200-400 Hz are visible in the plots: these instabilities are of the same type and expected frequency level as the typical hybrid rocket low frequency instability defined in [22]. However, it is also expected that 1L-mode and Helmholtz acoustic instabilities have occurred during the tests at frequencies well higher than 1000 Hz, thus at higher frequencies than the Nyquist one for the test setup used in this campaign. Therefore, the presence of aliasing signals in the test data cannot be completely excluded. It can also be concluded that the detected instabilities have no significant impact on performance, and seem to be much more closely related to the combustion pressure shifts (as explained in next Section) than the oxidizer mass flux.

Equations 1, 5 and 6 in [22] have been used to evaluate the expected frequency of different types of instabilities. Depending on the values used for the oxidizer mass flux (initial or final one) and the combustion temperature (from literature or from combustion reaction simulators), the following ranges of frequencies are obtained for test 9 (see Figure 10):

- Intrinsic low-frequency instability: 200 – 440 Hz
- Helmholtz instability: 1050 – 1550 Hz
- 1-L mode acoustic instability: 1950 – 2300 Hz

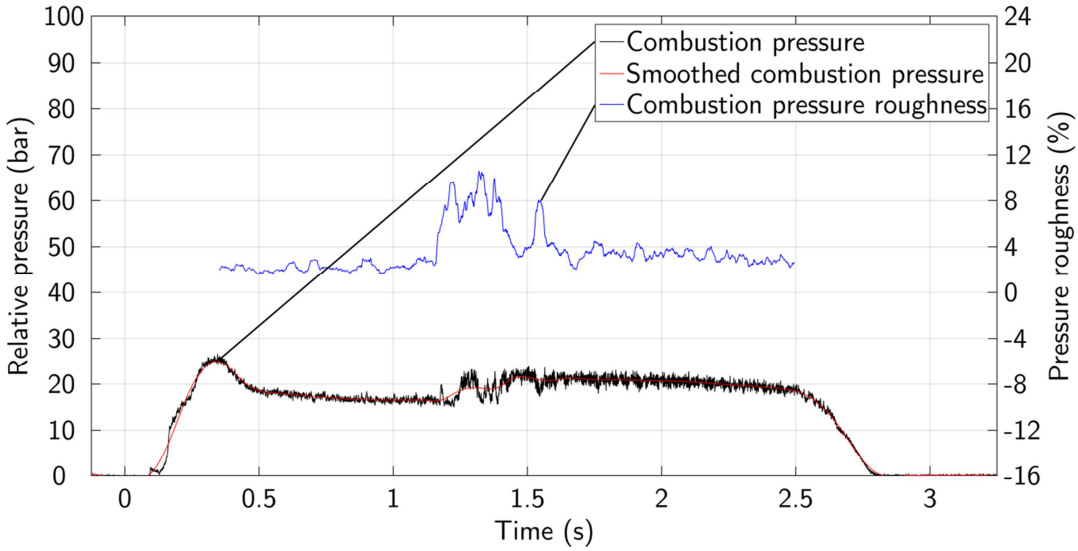

Fig. 8 Combustion roughness during Test 12, as a function of time

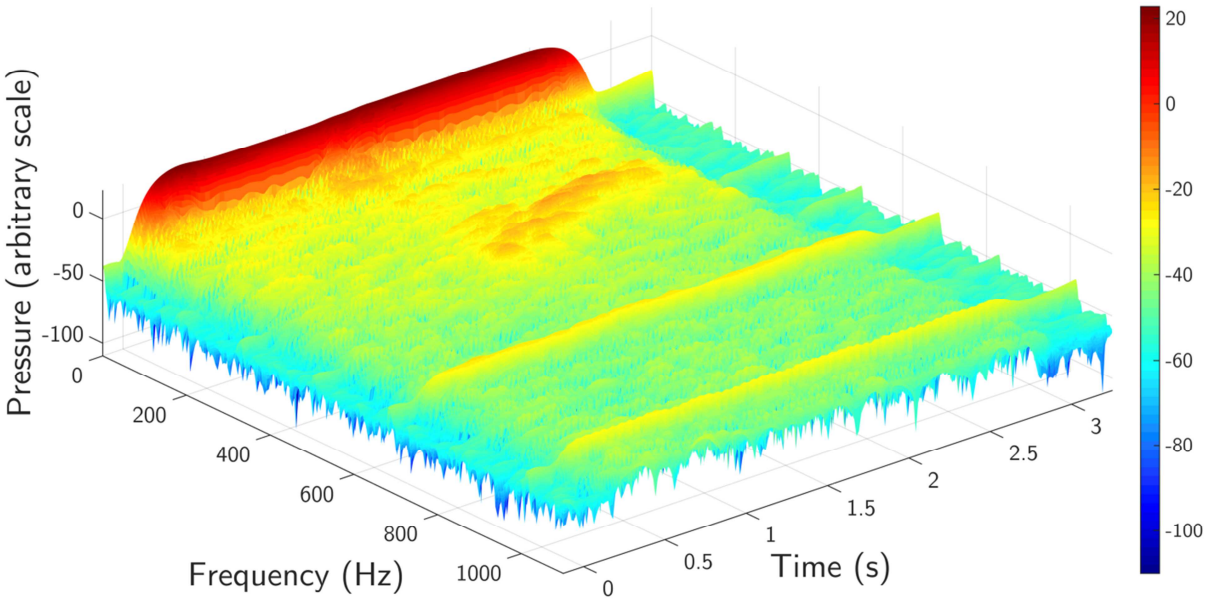

Fig. 9 Frequency spectrum of the combustion chamber pressure during Test 12

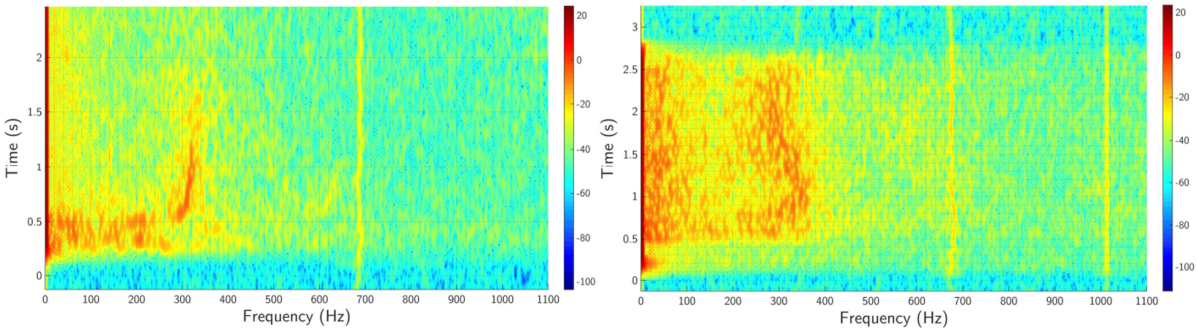

Fig. 10 Frequency spectra of the combustion chamber pressure during Test 9 (left) and Test 14 (right)

VII. Discussion

The most important phenomenon observed during the experimental campaign is the already mentioned spontaneous combustion pressure shift. The impact of this type of instability on the engine performance, as well as the role of the oxidizer mass flux on it, are discussed more in detail in this Section.

A. Injector Performance

As previously discussed, the injector plays an important role in the combustion behavior. It is therefore essential to assess the difference among the performance of the different injectors, before discussing the engine performance

itself. To this respect, the average feeding system pressure drop, injector pressure drop, and oxidizer mass flow are shown in Fig. 11 for all the performed tests.

The feeding system pressure drop of injector 2 is clearly higher than injector 1, and the one of injector 3 is higher than injector 2. The same applies to the oxidizer mass flow. There is no visible injector pressure drop difference between injectors 1 and 2, while for injector 3 the pressure drop is clearly lower than injectors 1 and 2, and even lower than the feeding system pressure drop. This means that in the case of injector 3 the flow is not choked at the injector but somewhere else in the feeding system. This is an undesirable condition since it reduces the injector upstream pressure stability, where the injector is not providing full isolation from the combustion chamber. The tests with failed ignition (Test 2, 8, 11 and 13) can be clearly distinguished by their much higher injector pressure drop but, due to the incorrect operational conditions under which they run and the absence of combustion in particular, the data related to these tests shall not be taken into account.

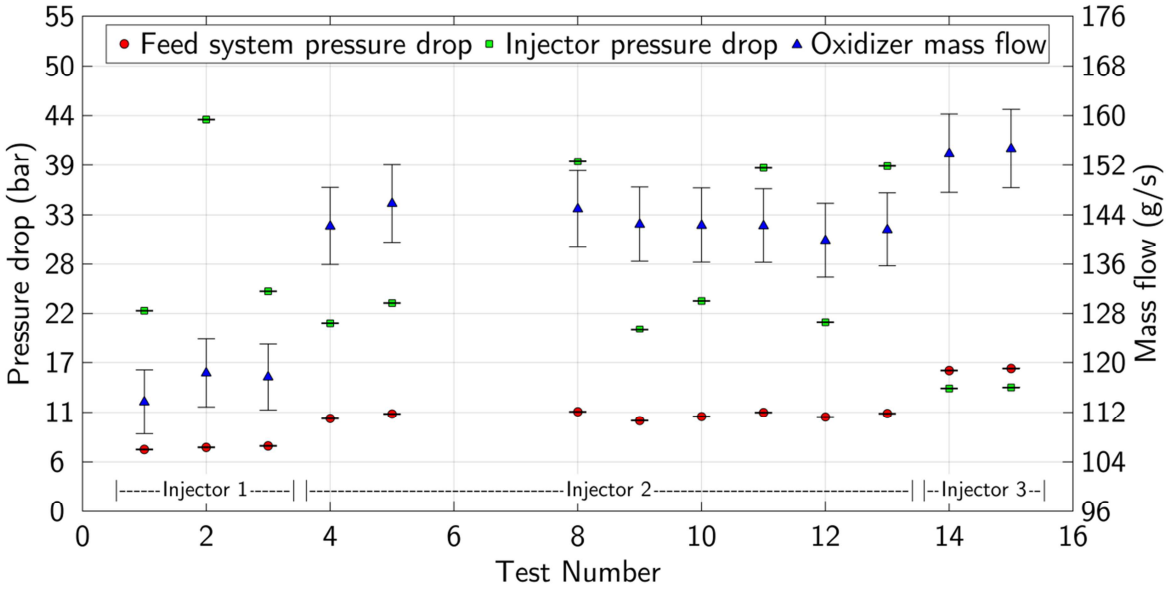

Fig. 11 Pressure drop over the feeding system, injector pressure drop and oxidizer mass flow measured in all the experimental campaign tests

B. Engine Performance

To determine the influence of the initial oxidizer mass flux on the engine performance, Fig. 12 shows the combustion efficiency (in terms of c^* efficiency) as a function of this parameter. By means of a statistical linear regression analysis it can be determined that there is a significant decrease in combustion efficiency with increasing

initial oxidizer mass flux. By analyzing the influence of all the involved parameters, it can be inferred that the decrease in combustion efficiency is caused by a combustion pressure decrease, as shown in Fig. 13. The figure also shows how this parameter changes with the three different injectors.

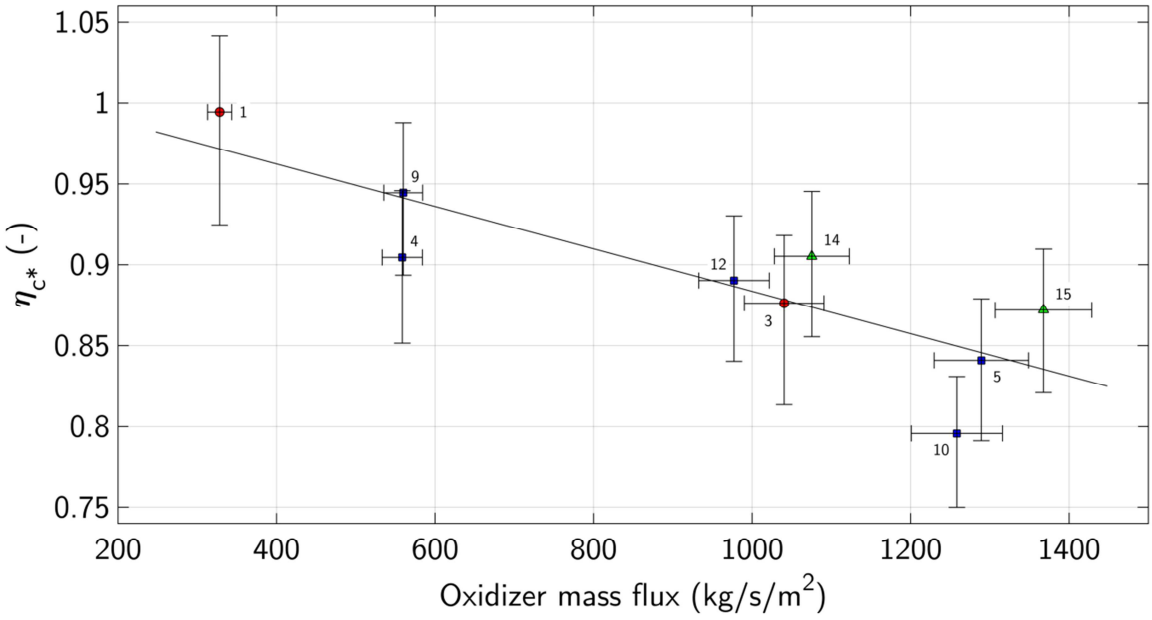

Fig. 12 Average combustion efficiency as a function of the initial oxidizer mass flux (the number close to each experimental point indicates the test to which it refers)

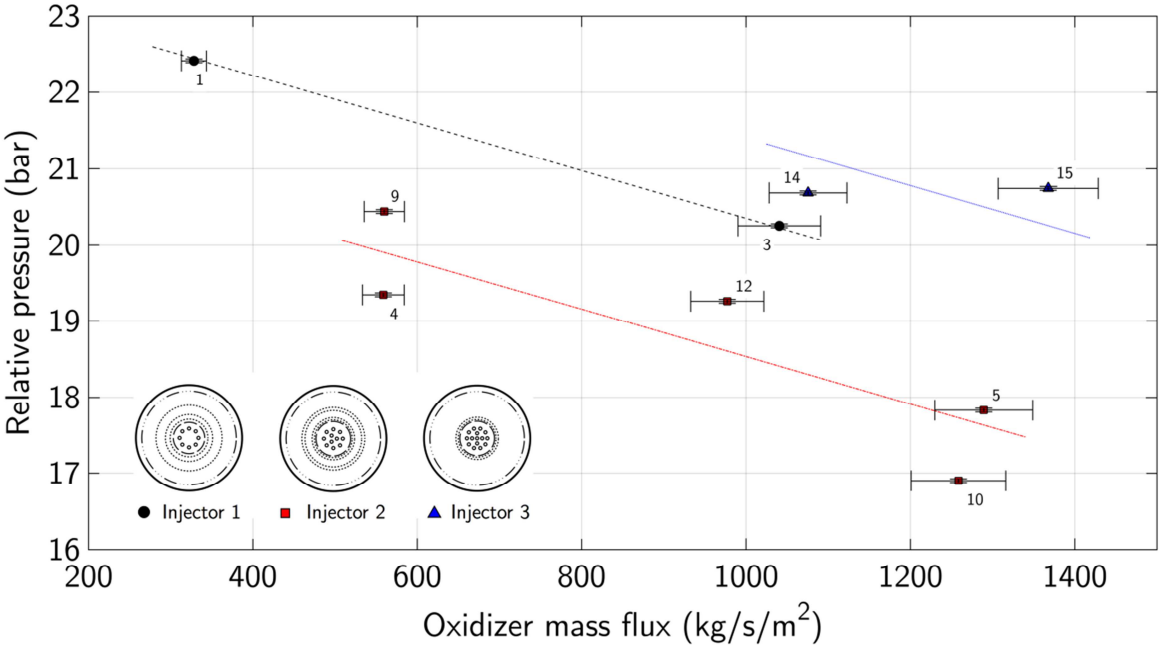

Fig. 13 Average combustion pressure as a function of the initial oxidizer mass flux, for the three different injector types (the number close to each experimental point indicates the test to which it refers)

C. Spontaneous Combustion Pressure Shifting

From what has been shown in previous sections, most of the tests exhibited sudden shifts in combustion pressure. These shifts are of such a magnitude that they can explain the significant difference in average combustion pressure between some of the tests. It is however also interesting to determine whether this phenomenon is related to the oxidizer mass flux and, if so, in which way.

As observed in Figs. 5 and 14, in all tests (with the exception of Test 1), a large combustion pressure shift occurs at around 0.5 seconds, regardless of the different oxidizer mass flux level and injector design at which they have been performed. In the tests with injector types 1 and 2, the combustion pressure seems to settle at around 30 bar initially but then drops to a significantly lower level, either gradually or suddenly, after around 0.5 seconds. To the contrary, for injector type 3, the combustion pressure initially settles at a lower level around 20 bar, and then shifts to a higher level (around 30 bar) after around 0.5 seconds. In tests 5, 10 and 12 the combustion pressure shifts back to a higher level sometimes after the middle of the burn. In tests 3, 4 and 9 the pressure does not return to a higher level after the initial drop after around 0.5 seconds. Tests 5 and 10, even if exactly the same engine configuration was used, show some difference in the combustion pressure behavior during the initial 0.5 seconds and in the time at which the combustion pressure starts to shift to a higher value again. In tests 14 and 15, upward and downward shifts seem to alternate rapidly. Although, towards the end of the burn it is less clear whether the alternating combustion pressure can be interpreted as shifts or as a more general combustion roughness.

From these observations, it can be concluded that the combustion pressure shifts are probably not mainly related to the initial oxidizer mass flux. Tests 3, 12 and 14, for instance, were conducted at similar values of the initial oxidizer mass flux but show a very different combustion behavior. Furthermore, the observed similarities and differences in the timing and magnitude of the shifts are difficult to explain by looking at the initial oxidizer mass flux only. To the contrary, it can be easily inferred that the injector design plays an important role on the combustion behavior.

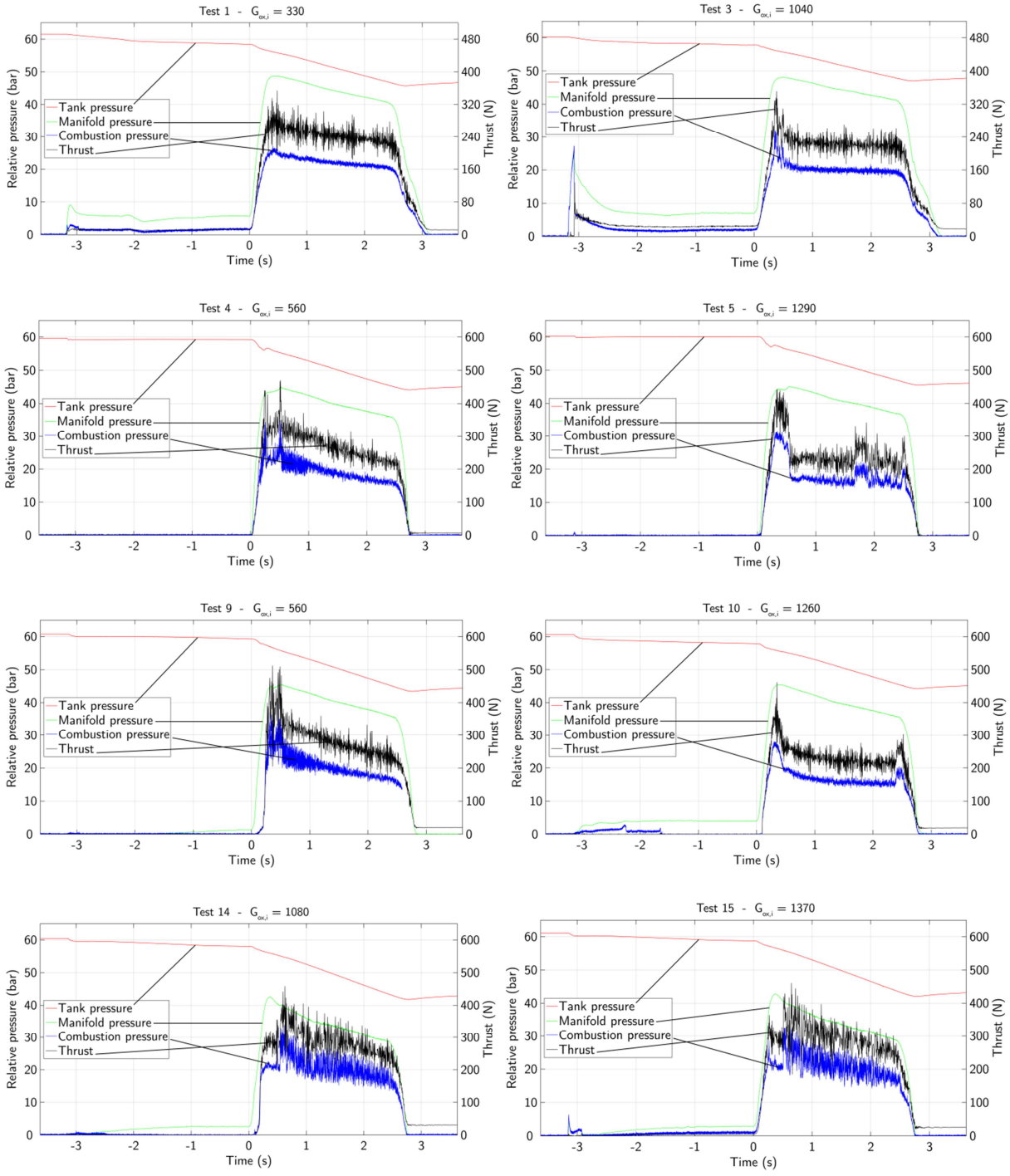

Fig. 14 Measured thrust and pressures in the tank, injector and chamber during various tests, as functions of time ($G_{ox,i}$ in kg/s·m^2)

A possible explanation for the spontaneous combustion pressure shifting can be found in Karabeyoglu and Dyer [23]. According to them, the operation of a hybrid rocket engine under certain conditions are usually characterized by multiple stable equilibrium points. Thus, the observed pressure shifts might be interpreted as switches from one stable mode (higher combustion efficiency and pressure) to another stable mode (lower combustion efficiency and pressure). It is easy to show that any other possible cause of combustion pressure changes is not applicable to this case. No clear variations of oxidizer mass flow rate and nozzle throat area could be observed during the tests or after each test. The regression rate of the solid fuel was not measured or analyzed during the test campaign, but any realistic variations of it would not be sufficient to explain the substantial changes in chamber pressure. Thus, the only possible explanation left is a variation in the combustion efficiency of the engine which, in turn, cannot be explained by other causes such as partial blow-off by high mass flux and can only be related to a coupling between the combustion efficiency and the injector performance.

The existence of multiple equilibrium points is attributed to the inverse relation of the combustion efficiency with the injector pressure drop. This can be physically explained by the fact that combustion becomes less efficient as the jet breakup distance increases as a result of injector pressure drop increase or of hydraulic flipping. To prevent the engine from having multiple stable equilibrium points, the injector pressure drop for efficient combustion has to be above a given critical value, which can in principle be estimated by means of a model described in [23].

D. Blow-off Limit

The first goal of this research was to find a blow-off limit for the tested engine or, in other words, the flammability limit in terms of oxidizer mass flux, where the steady state combustion can not be sustained.

Failed ignition only occurred twice during the experimental campaign. In both cases, at a relative low initial oxidizer mass flux of about 450 $kg/s \cdot m^2$ (test 11 and 13). These failures are thought to be related to either the igniter performance, the feeding system configuration, and/or the pre-combustion chamber design and the volume available to the recirculating flow rather than the oxidizer mass flux itself. Furthermore, spontaneous shifts to a lower combustion pressure level force the engine to work at an inefficient but stable operation point, and are not expected to be related to partial blow-off. Therefore, no certain blow-off limit could be found during the present research.

VIII. Conclusion

This study has been triggered by the well-known concept, universally accepted in open literature, that combustion stability and flame holding problems are expected to occur in hybrid rocket engines operating at mass flux levels above the 500-700 kg/s·m^2 range. A test setup and an experimental methodology have been developed to study these phenomena in the high oxidizer mass flux regime, and a total of 15 experiments have been performed on a N_2O-PMMA hybrid rocket engine with a nominal thrust level of 300 N, at initial oxidizer mass flux levels below 500, between 500 and 700, and above 700 kg/s·m^2.

No blow-off limit was found in the operating range up to 1370 kg/s·m^2. Higher mass flux levels could not be tested because of the limitations of the test setup. An inverse correlation has been found between the average combustion efficiency and the initial oxidizer mass flux, which is the result of an inverse correlation between the average combustion pressure and the initial oxidizer mass flux. The observed spontaneous combustion pressure shifts are a likely explanation for at least part of the differences in average combustion pressure. Furthermore, these combustion pressure shifts seem to be not related to the oxidizer mass flux.

The shifts can be explained by a theory that attributes this phenomenon to the existence of multiple stable equilibrium points of engine operation under certain conditions. According to this theory, the problem can be prevented, or at least limited, by keeping the injector pressure drop for the efficient combustion mode above a certain critical value for a given configuration.

Due to some test data limitations, such as a lack of instantaneous mass flow measurements, it was unfortunately not possible to determine whether this theory can explain all the observed combustion pressure shifts. Therefore it is still questionable whether a simple injector pressure drop increase would solve the problem, and it is not possible to determine whether there is a correlation between the combustion pressure shifts and the initial oxidizer mass flux. Consequently, it is also not possible to determine to what extent the observed worse engine performance has been actually caused by an oxidizer mass flux increase.

Future tests need to be planned to further understand the shifting phenomenon and how it can be eliminated or reduced. After eliminating this phenomenon, it will be possible to determine in an effective way how the oxidizer mass flux affects the engine performance and to assess whether it is actually useful to operate at mass flux levels higher than 650 kg/s·m^2 and, if so, under which design conditions. Finally, we recommend to study in detail the influence of different engine configurations, geometry and size, propellants and injector types.

Acknowledgments

This paper is based on the first author's Master thesis project at the Faculty of Aerospace Engineering of the Delft University of Technology. The research has been partly funded by Delft Aerospace Rocket Engineering (DARE), of which the first author is a member. Technical and operational support for the experiments was provided by members of the hybrid propulsion development team of DARE.

References

[1] Zilliac, G., and Karabeyoglu, M. A., "Hybrid Rocket Fuel Regression Rate Data and Modeling", *42nd AIAA/ASME/SAE/ASEE Joint Propulsion Conference and Exhibit*, AIAA 2006-4504, Sacramento, CA, 2006.

[2] Bettner, M., and Humble, R.W., *Polyethylene and Hydrogen Peroxide Hybrid Testing at the United States Air Force Academy*, 19990827 041, Air Force Academy, Colorado Springs, CO, 1998.

[3] Hertzelle, W.S,. and Waite, M. J., "Design of a Small H2O2-HTPB Hybrid Sounding Rocket Motor", AIAA, *34th Aerospace Sciences Meeting and Exhibit*, Reno, NV, 1996.

[4] Rao, D., Cai, G., Zhu, H., and Tian, H., "Design and Optimization of Variable Thrust Hybrid Rocket Motors for Sounding Rockets", *Science China – Technological Sciences*, Vol. 55, No. 1, 2012, pp. 125–135.

[5] Vilanova, C.Q., Da Cas, P.L.K., Barcelos M.N.D., and Veras C.A.G., "Multidisciplinary Design Optimization of a De-Boost Hybrid Motor for the Brazilian Recoverable Satellite", *2nd International Conference on Engineering Optimization*, Lisbon, Portugal, 2010.

[6] Zilliac, G., Waxman, B.S., Doran, E., Dyer, J., Karabeyoglu, M. A., and Cantwell, B., "Peregrine Hybrid Rocket Motor Ground Test Results, *48th AIAA/ASME/SAE/ASEE Joint Propulsion Conference & Exhibit*, AIAA 2012-4017, Atlanta, GA, 2012.

[7] Claflin, S.E., and Beckman, A.W., "Hybrid Propulsion Technology Program: Phase 1, volume 4", Final Report, RI/RD89-261, 1989.

[8] Wink, J., Knop, T., Huijsman, R., Powell, S., Samarawickrama K., Fraters, A., Werner, R., Becker, C., Lindeman, F., Ehlen, J., Cervone, A., and Zandbergen, B., "Test Campaign on a 10 kN Class Sorbitol-Based Hybrid Rocket Motor for the Stratos II Sounding Rocket", *Space Propulsion Conference*, SP2014-2969362, Cologne, Germany, 2014.

[9] Pastrone, D., "Approaches to Low Fuel Regression Rate in Hybrid Rocket Engines", *International Journal of Aerospace Engineering*, 2012, pp. 1–15.

[10] Chiaverini, M., "Review of Solid-Fuel Regression Rate Behavior in Classical and Nonclassical Hybrid Rocket Motors", *Progress in Astronautics and Aeronautics*, 218, 37, 2007.

[11] Muzzy, R.J., “Applied Hybrid Combustion Theory”, *AIAA/SAE 8th Joint Propulsion Specialist Conference*, AIAA 72-1143, New Orleans, LA, 1972.

[12] Netzer, D.W., and Bae W.E., *Hybrid Rocket Internal Ballistics*, No. CPIA-PUB-222, Chemical Propulsion Information Agency Laurel MD, 1972.

[13] Muzzy, R.J., Feemster, J.R., and Spangler, W.E., “The Design of a Hybrid Rocket Propulsion System”, *9th Liquid Propulsion Symposium*, St. Louis, MO, 1967.

[14] Wooldridge C.E., and Muzzy, R.J., “Internal Ballistic Considerations in Hybrid Rocket Design”, *Journal of Spacecraft and Rockets*, Vol. 4, No. 2, 1967, pp. 255–262.

[15] Marxman, G.A., Wooldridge, C.E., and Muzzy, R.J., “Investigation of Fundamental Phenomena in Hybrid Propulsion”, *Final Tech. Rept., Vol. I, Contract NOw 64-0659-c*, 1965.

[16] Elands, R., Dijkstra, F., and Zandbergen, B., “Experimental and Computational Flammability Limits in a Solid Fuel Ramjet”, AIAA paper n. 90-1964, 1990.

[17] Liou T.M., Lien W.Y., and Hwang P.W., “Flammability Limits and Probability Density Functions in Simulated Solid-Fuel Ramjet Combustors”, *Journal of Propulsion and Power*, Vol. 13, No. 5, 1997, pp. 643-650.

[18] Calzone, R.F., "Flammability Limits of a Solid Fuel Ramjet Combustor", *ICAS Proceedings*, Vol. 18, American Institute of Aeronautics and Astronautics, 1992.

[19] Prior, R., Fowler, D., and Mellor, A., “Engineering Design Models for Ramjet Efficiency and Lean Blowoff”, *AIAA/SAE/ASME/ASEE 26th Joint Propulsion Conference*, AIAA 90-2453, Orlando, FL, 1990.

[20] Boardman, T.A., Brinton, D.H., Carpenter, R.L., and Zoladz T.F., “An Experimental Investigation of Pressure Oscillations and Their Suppression in Subscale Hybrid Rocket Motors”, *31st AIAA/ASME/SAE/ASEE Joint Propulsion Conference and Exhibit*, AIAA 95-2689, San Diego, CA, 1995.

[21] Boardman, T.A., Carpenter R.L., and Claflin S.E., "A Comparative Study of the Effects of Liquid Versus Gaseous Oxygen Injection on Combustion Stability in 11-Inch-Diameter Hybrid Motors", AIAA Paper n. 97-2936, 1997.

[22] Carmicino C., “Acoustics, Vortex Shedding, and Low Frequency Dynamics Interaction in an Unstable Hybrid Rocket”, *Journal of Propulsion and Power*, Vol. 25, No. 6, 2009, pp. 1322–1335.

[23] Karabeyoglu A., and Dyer J., “Nonlinear Combustion in Hybrid Rockets - Explanation of Spontaneous Shifting in Motor Operation”, *45th AIAA/SAE/ASME/ASEE Joint Propulsion Conference and Exhibit*, AIAA 2009-5218, Denver, CO, 2009.